Shock structure due to stochastic forcing and the time reversal of nonlinear waves [1]

Jean-Pierre Fouque

Department of Mathematics, North Carolina State University, Raleigh NC 27695-8205.

Josselin Garnier [2]

Laboratoire de Statistique et Probabilités, Université Paul Sabatier, 118 Route de Narbonne, 31062 Toulouse Cedex 4, France.

André Nachbin [3]

Instituto de Matemática Pura e Aplicada, Est. D Castorina 110 , Jardim Botânico, Rio de Janeiro, RJ 22460-320, Brazil.

Abstract

This paper is concerned with the study of the deformation of a nonlinear pulse traveling in a random medium. We consider shallow water waves with a spatially random depth. We demonstrate that in the presence of properly scaled stochastic forcing the solution to the nonlinear conservation law is regularized leading to a viscous shock profile. This enables us to perform time-reversal experiments beyond the critical time for shock formation.

Key words: Nonlinear waves, inhomogeneous media, viscous shock, time reversal.
PACS: 47.35.+i, 42.25.Dd, 43.25.Ts, 43.60.Cg

Email addresses: fouque@math.ncsu.edu (Jean-Pierre Fouque), garnier@cict.fr (Josselin Garnier), nachbin@impa.br (André Nachbin).

[1] This work was supported by the MGSS program while the authors were visiting Stanford University and by ONR under grant N00014-02-1-0089. The authors would like to thank Vincenzo Casulli (Università di Trento, Italy) for the copy of his code (TRIM3D).

[2] The author acknowledges support from the program ACI-NIM-2003-94.

[3] This work was supported by CNPq/Brazil under grant 300368/96-8.

1 Introduction

In this paper we address the propagation of nonlinear waves in a disordered one-dimensional medium. We demonstrate that in the presence of properly scaled stochastic forcing the solution to the nonlinear conservation law is regularized leading to a viscous shock profile. More precisely, we consider a two-by-two hyperbolic system and we show that to leading order the transmitted wave is governed by a viscous Burgers equation. As a consequence of this regularization effect, time-reversal can be performed beyond the shock critical time.

The propagation of a linear pulse through a random medium has been extensively studied (see for instance the review [1]). In particular the O'Doherty Anstey theory predicts that if the pulse is observed in a Lagrangian frame that moves with a random velocity, then the pulse appears to retain its shape up a to a slow spreading and attenuation [20]. A rather convincing heuristic explanation of this phenomenon is given in [4]. The mathematical treatment of this issue is addressed in [4,3,6,15,16,2]. We have extended this theory to nonlinear waves by decomposing the solution of the perturbed system using the Riemann invariants of the unperturbed system. Using limit theorems and stochastic calculus we show that the right-going Riemann invariant satisfies a viscous Burgers equation. The apparent viscosity reads as a pseudo-differential operator imposed by the power spectral density of the random fluctuations.

Time-reversal refocusing for waves propagating in inhomogeneous media have been recently observed and studied experimentally in various contexts, e.g. ultrasound, underwater acoustics, see for instance the review [10]. Important potential applications have been proposed in various fields, for instance imaging [21,11] and communication [9]. A time-reversal mirror is, roughly speaking, a device which is capable of receiving a signal in time, keeping it in memory and sending it back into the medium in the reversed direction of time. The main effect is the refocusing of the scattered signal after time-reversal in a random medium. Surprisingly, the refocused pulse shape only depends on the statistical properties of the random medium, and not on the particular realization of the medium. The full mathematical understanding, meaning both modeling of the physical problem and derivation of the time-reversal effect, is a complex problem. The study of the one-dimensional linear case is now well understood [7,22,13]. In this paper we give an analysis of time-reversal of weakly nonlinear waves propagating in a one-dimensional disordered medium. The main result is that the regularization effect mentioned above enables us to perform time-reversal of the transmitted wave beyond the shock distance of the homogeneous problem.

This paper is organized as follows. In Section 2 we introduce the nonlinear

shallow water wave model with random depth together with the corresponding Riemann invariants. In Section 3 we derive the effective Burgers equation governing the evolution of the front pulse. We discuss the properties of this effective equation in Section 4. We study the time reversal of this pulse in Section 5. Section 6 is devoted to full numerical simulations of the system.

2 Shallow water waves with random depth

The shallow water equations are given by [8]

$$\frac{\partial \eta}{\partial t} + \frac{\partial (1 + \varepsilon h + \alpha \eta) u}{\partial x} = 0, \tag{1}$$

$$\frac{\partial u}{\partial t} + \frac{\partial \eta}{\partial x} + \alpha u \frac{\partial u}{\partial x} = 0, \tag{2}$$

where η is the free surface elevation and u is the horizontal velocity component. The fluid body is given by $H(x,t) = 1 + \varepsilon h(x) + \alpha \eta(x,t)$. The parameter α is the ratio of the typical wave amplitude over the mean depth. It governs the strength of the nonlinearity. It is assumed to be small. The parameter ε is the order of magnitude of the fluctuations of the depth, which are described by the stationary zero-mean random process $h(x)$. It is assumed to be small. We shall see that the suitable scaling between ε and α to exhibit the interplay between these two effects is

$$\alpha = \varepsilon^2 \alpha_0 \tag{3}$$

where α_0 is the normalized nonlinear parameter which is of order 1. In the physical world it means that the amplitude of the wave elevation is smaller than the amplitude of the fluctuations of the bottom, which is itself smaller than the mean depth. Let us introduce the "deterministic" local propagation speed

$$c = \sqrt{1 + \alpha \eta}, \tag{4}$$

which does not include the term εh, but it is nevertheless random through the term $\alpha \eta$. We can reformulate the above equations in terms of c and u to obtain

$$\frac{\partial c}{\partial t} + \frac{\alpha}{2} c \frac{\partial u}{\partial x} + \alpha u \frac{\partial c}{\partial x} + \frac{\alpha \varepsilon}{2c} \frac{\partial h u}{\partial x} = 0, \tag{5}$$

$$\frac{\partial u}{\partial t} + \alpha u \frac{\partial u}{\partial x} + \frac{2}{\alpha} \frac{\partial c}{\partial x} = 0. \tag{6}$$

We define the Riemann invariants

$$A(x,t) = \frac{\alpha u - 2c + 2}{\alpha}, \tag{7}$$

$$B(x,t) = \frac{\alpha u + 2c - 2}{\alpha}, \tag{8}$$

which satisfy

$$\frac{\partial A}{\partial t} + (\alpha u - c)\frac{\partial A}{\partial x} = \varepsilon \frac{1}{c}\frac{\partial hu}{\partial x}, \tag{9}$$

$$\frac{\partial B}{\partial t} + (\alpha u + c)\frac{\partial B}{\partial x} = -\varepsilon \frac{1}{c}\frac{\partial hu}{\partial x}. \tag{10}$$

Note that in absence of random perturbations $\varepsilon = 0$, the two Riemann invariants are constant along different characteristics. Taking into account the fact that $\alpha = \alpha_0 \varepsilon^2$, we can rewrite these equations in terms of A and B only:

$$\frac{\partial A}{\partial t} + (-1 + \alpha \frac{3A + B}{4})\frac{\partial A}{\partial x} = \frac{\varepsilon}{2}\frac{\partial h(A+B)}{\partial x}\frac{1}{1 + \alpha(B-A)/4}, \tag{11}$$

$$\frac{\partial B}{\partial t} + (1 + \alpha \frac{A + 3B}{4})\frac{\partial B}{\partial x} = -\frac{\varepsilon}{2}\frac{\partial h(A+B)}{\partial x}\frac{1}{1 + \alpha(B-A)/4}. \tag{12}$$

If the nonlinearity parameter is small $\alpha \ll 1$, we get back the standard left- and right-going modes (A and B, respectively) of the hyperbolic linear system.

REMARK. *We could have chosen to consider the true "random" local propagation speed*

$$\check{c} = \sqrt{1 + \alpha\eta + \varepsilon h}.$$

The Riemann invariants are still defined by

$$\check{A}(x,t) = \frac{\alpha u - 2\check{c} + 2}{\alpha}, \qquad \check{B}(x,t) = \frac{\alpha u + 2\check{c} - 2}{\alpha}.$$

They satisfy the following system of equations

$$\frac{\partial \check{A}}{\partial t} + (-1 + \alpha \frac{3\check{A} + \check{B}}{4})\frac{\partial \check{A}}{\partial x} = \frac{\varepsilon}{\alpha}\frac{\partial h}{\partial x},$$

$$\frac{\partial \check{B}}{\partial t} + (1 + \alpha \frac{\check{A} + 3\check{B}}{4})\frac{\partial \check{B}}{\partial x} = -\frac{\varepsilon}{\alpha}\frac{\partial h}{\partial x}.$$

This system seems simpler as the random noise is additive, and not multiplicative. However, we must remember that $\alpha = \varepsilon^2 \alpha_0$, so the perturbation is already singular in the microscopic scale (t and x of order 1), which leads to enhanced complications in the macroscopic scales (t and x of order ε^{-2}). That

is why we have adopted the formulation in terms of the "deterministic" local propagation speed c.

We can rewrite the evolution equations for A and B in the following way, up to terms of order ε^3,

$$\frac{\partial}{\partial x}\begin{pmatrix} A \\ B \end{pmatrix} = Q(x)\frac{\partial}{\partial t}\begin{pmatrix} A \\ B \end{pmatrix} - \varepsilon\frac{h'}{2}\begin{pmatrix} 1 & 1 \\ 1 & 1 \end{pmatrix}\begin{pmatrix} A \\ B \end{pmatrix} + \varepsilon^2\frac{\alpha_0}{4}\begin{pmatrix} 3A+B & 0 \\ 0 & A+3B \end{pmatrix}\frac{\partial}{\partial t}\begin{pmatrix} A \\ B \end{pmatrix} + O(\varepsilon^3), \tag{13}$$

where h' stands for the spatial derivative of h and

$$Q(x) = \frac{1}{1+\varepsilon h}\begin{pmatrix} 1+\varepsilon\frac{h}{2} & \varepsilon\frac{h}{2} \\ -\varepsilon\frac{h}{2} & -1-\varepsilon\frac{h}{2} \end{pmatrix} \tag{14}$$

The system is completed by the initial condition corresponding to a right-going wave incoming from the homogeneous half-space $x < 0$

$$A(x,t) = 0, \quad B(x,t) = f(t-x), \quad t < 0,$$

where the function f is compactly supported in $(-\infty, 0)$.

3 Derivation of the effective equation for the front pulse

In this section we perform a series of transformations to rewrite the evolution equations of the modes by centering along the characteristic of the right-going mode. We will then obtain a lower-triangular system that can be integrated more easily. In a second step we shall apply an averaging theorem to this system to establish an effective nonlinear equation for the front pulse.

The eigenvalues of the matrix $Q(x)$ are $\pm\gamma^\varepsilon(x)$ with

$$\gamma^\varepsilon(x) = \frac{1}{\sqrt{1+\varepsilon h}}. \tag{15}$$

We introduce the unitary matrix U

$$U = \sqrt{\frac{2+\varepsilon h+2\sqrt{1+\varepsilon h}}{4+2\varepsilon h}} \begin{pmatrix} 1 & -\frac{\varepsilon h}{2+\varepsilon h+2\sqrt{1+\varepsilon h}} \\ -\frac{\varepsilon h}{2+\varepsilon h+2\sqrt{1+\varepsilon h}} & 1 \end{pmatrix} \tag{16}$$

which is such that

$$UQU^{-1} = \gamma^{\varepsilon}(x) \begin{pmatrix} 1 & 0 \\ 0 & -1 \end{pmatrix}.$$

We then introduce the modified modes

$$\begin{pmatrix} A_1 \\ B_1 \end{pmatrix} = U \begin{pmatrix} A \\ B \end{pmatrix} \tag{17}$$

They satisfy

$$\begin{aligned} \frac{\partial}{\partial x} \begin{pmatrix} A_1 \\ B_1 \end{pmatrix} =& \gamma^{\varepsilon} \begin{pmatrix} 1 & 0 \\ 0 & -1 \end{pmatrix} \frac{\partial}{\partial t} \begin{pmatrix} A_1 \\ B_1 \end{pmatrix} - \varepsilon \frac{h'}{4} \begin{pmatrix} 2 & 1 \\ 1 & 2 \end{pmatrix} \begin{pmatrix} A_1 \\ B_1 \end{pmatrix} \\ &+\varepsilon^2 \frac{\alpha_0}{4} \begin{pmatrix} 3A_1+B_1 & 0 \\ 0 & A_1+3B_1 \end{pmatrix} \frac{\partial}{\partial t} \begin{pmatrix} A_1 \\ B_1 \end{pmatrix} + O(\varepsilon^3). \end{aligned} \tag{18}$$

We shall perform the change of variable

$$z(x) = \int_0^x \gamma^{\varepsilon}(x')dx' \tag{19}$$

and we again modify slightly the modes to simplify the equation:

$$\begin{pmatrix} A_2 \\ B_2 \end{pmatrix}(z,t) = \begin{pmatrix} A_1 \\ B_1 \end{pmatrix}(x(z),t) \exp\left(\varepsilon \frac{h(x(z))}{2}\right). \tag{20}$$

Note that $\frac{h'(x(z))}{\gamma(x(z))} = \frac{d}{dz}h(x(z))$. We still denote this quantity by h', so A_2 and B_2 satisfy

$$\frac{\partial}{\partial z} \begin{pmatrix} A_2 \\ B_2 \end{pmatrix} = \begin{pmatrix} 1 & 0 \\ 0 & -1 \end{pmatrix} \frac{\partial}{\partial t} \begin{pmatrix} A_2 \\ B_2 \end{pmatrix} - \varepsilon \frac{h'}{4} \begin{pmatrix} 0 & 1 \\ 1 & 0 \end{pmatrix} \begin{pmatrix} A_2 \\ B_2 \end{pmatrix}$$

$$+\varepsilon^2\frac{\alpha_0}{4}\begin{pmatrix}3A_2+B_2 & 0\\ 0 & A_2+3B_2\end{pmatrix}\frac{\partial}{\partial t}\begin{pmatrix}A_2\\ B_2\end{pmatrix}+O(\varepsilon^3). \tag{21}$$

We consider the reference frame that moves with the right-going mode B_2

$$\tau = t - z, \tag{22}$$

so that the equation now reads

$$\begin{aligned}\frac{\partial}{\partial z}\begin{pmatrix}A_2\\ B_2\end{pmatrix} &= \begin{pmatrix}2 & 0\\ 0 & 0\end{pmatrix}\frac{\partial}{\partial \tau}\begin{pmatrix}A_2\\ B_2\end{pmatrix} - \varepsilon\frac{h'}{4}\begin{pmatrix}0 & 1\\ 1 & 0\end{pmatrix}\begin{pmatrix}A_2\\ B_2\end{pmatrix}\\ &\quad +\varepsilon^2\frac{\alpha_0}{4}\begin{pmatrix}3A_2+B_2 & 0\\ 0 & A_2+3B_2\end{pmatrix}\frac{\partial}{\partial \tau}\begin{pmatrix}A_2\\ B_2\end{pmatrix}+O(\varepsilon^3).\end{aligned} \tag{23}$$

The equation for B_2 can be integrated as

$$B_2(z,\tau) = \int_0^z S_B(y,\tau)dy + f(\tau), \tag{24}$$

$$S_B(y,\tau) = -\varepsilon\frac{h'(y)}{4}A_2(y,\tau) + \varepsilon^2\frac{\alpha_0}{4}(A_2+3B_2)\frac{\partial B_2}{\partial \tau}(y,\tau) + O(\varepsilon^3). \tag{25}$$

Note that we consider propagation distance z of order ε^{-2}, but as we are interested in the front pulse we only consider local times τ of order 1, lying in some interval $[0,T]$ with fixed T.

The equation for A_2 can be integrated as

$$A_2(z,\tau) = -\frac{1}{2}\int_0^\tau S_A(z+\frac{\tau-s}{2},s)ds, \tag{26}$$

$$S_A(z,s) = -\varepsilon\frac{h'(z)}{4}B_2(z,s) + \varepsilon^2\frac{\alpha_0}{4}(3A_2+B_2)\frac{\partial A_2}{\partial \tau}(z,s) + O(\varepsilon^3), \tag{27}$$

which allows us to claim that

$$\sup_{z\in[0,L/\varepsilon^2],\tau\in[0,T]}|A_2(z,\tau)| \le K\varepsilon \tag{28}$$

and

$$\sup_{z\in[0,L/\varepsilon^2],\tau\in[0,T]}|\frac{\partial A_2}{\partial \tau}(z,\tau)| \le K\varepsilon. \tag{29}$$

Furthermore we can substitute the integral representation of A_2 into the one of B_2

$$B_2(z,\tau) = f(\tau) - \frac{\varepsilon^2}{32}\int_0^z h'(y)\int_0^\tau h'(y+\frac{\tau-s}{2})B_2(y+\frac{\tau-s}{2},s)dsdy$$
$$+\varepsilon^2\frac{3\alpha_0}{4}\int_0^z B_2\frac{\partial B_2}{\partial\tau}(y,\tau)dy + O(\varepsilon^3(1+z)). \tag{30}$$

Note that we have eliminated the terms $\varepsilon^2 A_2\partial_\tau B_2$, $\varepsilon^2 A_2\partial_\tau A_2$, $\varepsilon^2 B_2\partial_\tau A_2$, as they are of order ε^3 and are negligible for propagation distance of order ε^{-2}.

We introduce

$$B_2^\varepsilon(z,\tau) = B_2(\frac{z}{\varepsilon^2},\tau)$$

which satisfies

$$B_2^\varepsilon(z,\tau) = f(\tau) - \frac{1}{32}\int_0^z h'(\frac{y}{\varepsilon^2})\int_0^\tau h'(\frac{y}{\varepsilon^2}+\frac{\tau-s}{2})B_2^\varepsilon(y+\varepsilon^2\frac{\tau-s}{2},s)dsdy$$
$$+\frac{3\alpha_0}{4}\int_0^z B_2^\varepsilon\frac{\partial B_2^\varepsilon}{\partial\tau}(y,\tau)dy + O(\varepsilon). \tag{31}$$

By applying the Khasminskii's averaging theorem [14], we get that B_2^ε converges to $\tilde{B}_2$ solution of

$$\tilde{B}_2(z,\tau) = f(\tau) - \frac{1}{16}\int_0^z \Lambda\tilde{B}_2(y,\tau)dy + \frac{3\alpha_0}{4}\int_0^z \tilde{B}_2\frac{\partial\tilde{B}_2}{\partial\tau}(y,\tau)dy, \tag{32}$$

where the operator Λ is

$$\Lambda F(\tau) = \frac{1}{2}\int_0^\tau \phi_1(\frac{s}{2})F(\tau-s)ds = \left[\frac{1}{2}\phi_1\left(\frac{\cdot}{2}\right)\mathbf{1}_{[0,\infty)}(\cdot)\right] * F(\tau), \tag{33}$$
$$\phi_1(y) = \mathbb{E}[h'(z)h'(z+y)]. \tag{34}$$

In the Fourier domain

$$\int_{-\infty}^{\infty}\Lambda f(\tau)e^{i\omega\tau}d\tau = b_1(2\omega)\int_{-\infty}^{\infty} f(\tau)e^{i\omega\tau}d\tau, \tag{35}$$
$$b_1(\omega) = \int_0^\infty \phi_1(\tau)e^{i\omega\tau}d\tau, \tag{36}$$

and it is straightforward to check by integrating by parts that

$$b_1(\omega) = -i\omega\phi_0(0) + \omega^2 b_0(\omega), \tag{37}$$

$$b_0(\omega) = \int_0^\infty \phi_0(y) e^{i\omega y} dy, \tag{38}$$

$$\phi_0(y) = \mathbb{E}[h(z)h(z+y)]. \tag{39}$$

Accordingly,

$$\frac{\partial \tilde{B}_2}{\partial z} = -\frac{\phi_0(0)}{8}\frac{\partial \tilde{B}_2}{\partial \tau} + \mathcal{L}\tilde{B}_2 + \frac{3\alpha_0}{4}\tilde{B}_2\frac{\partial \tilde{B}_2}{\partial \tau}, \tag{40}$$

where $\mathcal{L}$ is a pseudo-differential operator. $\mathcal{L}$ behaves like a diffusion for small frequencies, but it decays to zero for high-frequencies signals. Its symbol is

$$\mathcal{L} = -\frac{b_0(2D)D^2}{4}.$$

In terms of the true mode B, we have to take care of the change of variable $x \mapsto z(x)$. In the macroscopic scales

$$z(\frac{x}{\varepsilon^2}) = \frac{x}{\varepsilon^2} - \frac{\varepsilon}{2}\int_0^{\frac{x}{\varepsilon^2}} h(x')dx' + \frac{\varepsilon^2}{8}\int_0^{\frac{x}{\varepsilon^2}} h(x')^2 dx' + O(\varepsilon), \tag{41}$$

so that it converges as

$$z(\frac{x}{\varepsilon^2}) - \frac{x}{\varepsilon^2} \overset{\varepsilon\to 0}{\longrightarrow} \frac{1}{\sqrt{2}}\sqrt{b_0(0)}W_x + \frac{1}{8}\phi_0(0)x, \tag{42}$$

where W_x is a standard Brownian motion. We can then state the following proposition.

Proposition 3.1 *The front pulse* $B^\varepsilon(x,\tau) := B(x/\varepsilon^2, \tau + x/\varepsilon^2)$, $x \in [0,L]$, $\tau \in [0,T]$, *converges to* $\tilde{B}$ *solution of*

$$\tilde{B}(x,\tau) = \tilde{B}_0\left(x, \tau - \frac{\sqrt{b_0(0)}}{\sqrt{2}}W_x - \frac{\phi_0(0)}{4}x\right), \tag{43}$$

$$\frac{\partial \tilde{B}_0}{\partial x} = \mathcal{L}\tilde{B}_0 + \frac{3\alpha_0}{4}\tilde{B}_0\frac{\partial \tilde{B}_0}{\partial \tau}, \tag{44}$$

$$\tilde{B}_0(0,\tau) = f(\tau). \tag{45}$$

4 Analysis of the equation for the front pulse

In this section we analyse the main properties of the effective equation for the front pulse. The important function that imposes the dynamics is

$$b_0(\omega) = \int_0^\infty \mathbb{E}[h(0)h(x)] \exp(i\omega x) dx$$

Note that $b_0(0)$ is proportional to the power spectral density of the random process h and is therefore a nonnegative real number. We have proved that $B(\frac{x}{\varepsilon^2}, \frac{x}{\varepsilon^2} + t)$ converges to $\tilde{B}$ given by (43-44). The Brownian motion W_x corresponds to a random time shift and $\mathcal{L}$ is a pseudo-differential operator that models the pulse spreading imposed by the random fluctuations of the bottom. $\mathcal{L}$ behaves like a diffusion for small frequencies, but it decays to zero for high-frequencies. Its symbol is

$$\mathcal{L} = -\frac{b_0(2D)D^2}{4}.$$

Note that the effective equation for the front pulse depends both on randomness (through the function b_0) and on nonlinearity (through the parameter α_0).

The pseudo-spectral operator $\mathcal{L}$ can be divided into two parts

$$\mathcal{L} = \mathcal{L}_r + \mathcal{L}_i, \tag{46}$$

$$\mathcal{L}_r = -\frac{b_r(2D)D^2}{4}, \tag{47}$$

$$\mathcal{L}_i = -\frac{ib_i(2D)D^2}{4}, \tag{48}$$

where b_r and b_i are respectively the real and imaginary part of b_0

$$b_r(\omega) = \int_0^\infty \mathbb{E}[h(0)h(x)] \cos(\omega x) dx, \tag{49}$$

$$b_i(\omega) = \int_0^\infty \mathbb{E}[h(0)h(x)] \sin(\omega x) dx. \tag{50}$$

In particular b_r is proportional to the power spectral density of the random process h. $\mathcal{L}_r$ can be described as an effective diffusion operator, while $\mathcal{L}_i$ is an effective dispersion operator, since it preserves the energy.

Let us address the case where the power spectral density of the process h can be considered as constant over the spectral range of f: $b_0(\omega) \equiv b_0$. This arises

if the typical wavelength of the pulse is larger than the correlation radius of the medium. In such a case the early steps of the effective evolution equation is that of the viscous Burgers equation

$$\frac{\partial \tilde{B}_0}{\partial x} = b_0 \frac{\partial^2 \tilde{B}_0}{\partial t^2} + \frac{3\alpha_0}{4} \tilde{B}_0 \frac{\partial \tilde{B}_0}{\partial t}. \tag{51}$$

However new frequencies are generated by the nonlinear term, that may fall in the tail of the function b_0. Then the last equation may eventually fail describing exactly the dynamics of the front pulse, and one must consider the true equation with the pseudo-differential operator.

The viscous Burgers equation (51) supports self-similar waves or even traveling waves as shown in [24, Chapter 4]. This means that the generalized O'Doherty-Anstey theory in a nonlinear scenario is not necessarily associated with attenuation. In a linear framework the effective viscosity generated by the random fluctuations always give rise to attenuation, but a nonlinearity can compensate for it and even produces a stable traveling wave. A simple example is the dam-breaking problem, where an initial step propagates into the random medium. The corresponding traveling wave is given in [24, Section 4.3].

5 Time reversal of the front pulse

5.1 Time reversal setup

The time reversal procedure consists in recording the transmitted signal at $z = L/\varepsilon^2$ over the time interval $[L/\varepsilon^2 + t_0, L\varepsilon^2 + t_1]$. A piece of the recorded signal is cut using a cut-off function $s \mapsto G_{t_0,t_1}(s - L/\varepsilon^2)$ where the support of G_{t_0,t_1} is included in $[t_0, t_1]$:

$$B^{\varepsilon}_{cut}(t) = B(x = \frac{L}{\varepsilon^2}, \frac{L}{\varepsilon^2} + t) G_{t_0,t_1}(t).$$

One then time reverses that piece of signal and send it back into the same medium by changing the sign of the velocity. From the expression of the Riemann invariants (7-8), the left going mode sent back is given by

$$C(x = \frac{L}{\varepsilon^2}, t) = -B(x = \frac{L}{\varepsilon^2}, \frac{L}{\varepsilon^2} + t_1 - t) G_{t_0,t_1}(t_1 - t).$$

In the time reversal experiment, the left-going mode is denoted by C and the right-going mode by D:

$$C(x,t) = \frac{\alpha u - 2c + 2}{\alpha}, \qquad D(x,t) = \frac{\alpha u + 2c - 2}{\alpha}.$$

REMARK. *To record the transmitted signal, we do not need to record both the elevation η and the velocity u. If we record only η, then we know the expression of u because we know that it is a right-going mode:*

$$u = \frac{2\sqrt{1+\alpha\eta} - 2}{\alpha}.$$

Furthermore, to re-emit the signal $C(x = \frac{L}{\varepsilon^2}, t)$, we do note need to generate both the elevation and the velocity. Indeed, if we generate for instance twice the elevation with a zero velocity, then this input pulse will split into a right-going mode, that will go to the right without coming back, and a left-going mode that is exactly the desired $C(x = \frac{L}{\varepsilon^2}, t)$.

The modes C and D satisfy

$$\begin{aligned}\frac{\partial}{\partial x}\begin{pmatrix} C \\ D \end{pmatrix} = & Q(x)\frac{\partial}{\partial t}\begin{pmatrix} C \\ D \end{pmatrix} - \varepsilon\frac{h'}{2}\begin{pmatrix} 1 & 1 \\ 1 & 1 \end{pmatrix}\begin{pmatrix} C \\ D \end{pmatrix} \\ & + \varepsilon^2\frac{\alpha_0}{4}\begin{pmatrix} 3C+D & 0 \\ 0 & C+3D \end{pmatrix}\frac{\partial}{\partial t}\begin{pmatrix} C \\ D \end{pmatrix} + O(\varepsilon^3), \end{aligned} \tag{52}$$

with the initial condition for $x > L/\varepsilon^2$:

$$C(x,t) = g^\varepsilon(t - x + \frac{L}{\varepsilon^2}), \qquad D(x,t) = 0, \quad t < 0.$$

Note that g^ε is compactly supported in $(0,\infty)$:

$$g^\varepsilon(t) = -B(x = \frac{L}{\varepsilon^2}, \frac{L}{\varepsilon^2} + t_1 - t)G_{t_0,t_1}(t_1 - t). \tag{53}$$

The goal of this section is to determine the shape of the transmitted wave at $x = 0$ around the expected arrival time $L/\varepsilon^2 + t_1$:

$$C^\varepsilon_{tr}(t) = C(x = 0, \frac{L}{\varepsilon^2} + t_1 + t). \tag{54}$$

Fig. 1. Forward scattering problem.

Fig. 2. Time reversal setup.

5.2 Derivation of the effective for the refocused pulse

As in Section 3 we shall rewrite the evolution of the time-reverted wave by centering along the characteristic of the left-going mode. Here we shall obtain an upper triangular system. The integration and averaging follow the same lines as in Section 3.

We introduce the modified modes

$$\begin{pmatrix} C_2 \\ D_2 \end{pmatrix}(z,t) = U \begin{pmatrix} C \\ D \end{pmatrix}(x(z),t) \exp\left(\varepsilon \frac{h(x(z))}{2}\right) \tag{55}$$

which satisfy

$$\begin{aligned} \frac{\partial}{\partial z}\begin{pmatrix} C_2 \\ D_2 \end{pmatrix} = \begin{pmatrix} 1 & 0 \\ 0 & -1 \end{pmatrix} \frac{\partial}{\partial t}\begin{pmatrix} C_2 \\ D_2 \end{pmatrix} - \varepsilon \frac{h'}{4}\begin{pmatrix} 0 & 1 \\ 1 & 0 \end{pmatrix}\begin{pmatrix} C_2 \\ D_2 \end{pmatrix} \\ + \varepsilon^2 \frac{\alpha_0}{4}\begin{pmatrix} 3C_2 + D_2 & 0 \\ 0 & C_2 + 3D_2 \end{pmatrix} \frac{\partial}{\partial t}\begin{pmatrix} C_2 \\ D_2 \end{pmatrix} + O(\varepsilon^3). \end{aligned} \tag{56}$$

We consider the reference frame that moves with the left-going mode C_2

$$\tau = t + z - z(\frac{L}{\varepsilon^2}), \tag{57}$$

so that the equation now reads

$$\frac{\partial}{\partial z}\begin{pmatrix} C_2 \\ D_2 \end{pmatrix} = \begin{pmatrix} 0 & 0 \\ 0 & -2 \end{pmatrix}\frac{\partial}{\partial \tau}\begin{pmatrix} C_2 \\ D_2 \end{pmatrix} - \varepsilon\frac{h'}{4}\begin{pmatrix} 0 & 1 \\ 1 & 0 \end{pmatrix}\begin{pmatrix} C_2 \\ D_2 \end{pmatrix}$$
$$+\varepsilon^2\frac{\alpha_0}{4}\begin{pmatrix} 3C_2 + D_2 & 0 \\ 0 & C_2 + 3D_2 \end{pmatrix}\frac{\partial}{\partial \tau}\begin{pmatrix} C_2 \\ D_2 \end{pmatrix} + O(\varepsilon^3). \qquad (58)$$

Integrating the equation for D_2 along its characteristic and substituting into the integral representation of C_2 establishes that, for $z \in [0, z(L/\varepsilon^2)]$,

$$C_2(z,\tau) = g^\varepsilon(\tau) - \frac{\varepsilon^2}{32}\int_z^{z(\frac{L}{\varepsilon^2})} h'(y)\int_0^\tau h'(y - \frac{\tau - s}{2})C_2(y - \frac{\tau - s}{2}, s)dsdy$$
$$-\varepsilon^2\frac{3\alpha_0}{4}\int_z^{z(\frac{L}{\varepsilon^2})} C_2\frac{\partial C_2}{\partial \tau}(y,\tau)dy + O(\varepsilon). \qquad (59)$$

Introducing

$$C_3(z,\tau) = C_2(z(\frac{L}{\varepsilon^2}) - z, \tau),$$

we get the equation

$$C_3(z,\tau) = g^\varepsilon(\tau) - \frac{\varepsilon^2}{32}\int_0^z\int_0^\tau \Big[h'(z(\frac{L}{\varepsilon^2}) - y)\times$$
$$h'(z(\frac{L}{\varepsilon^2}) - y - \frac{\tau - s}{2})C_3(y - \frac{\tau - s}{2}, s)\Big]\, dsdy$$
$$-\varepsilon^2\frac{3\alpha_0}{4}\int_0^z C_3\frac{\partial C_3}{\partial \tau}(y,\tau)dy + O(\varepsilon).$$

The refocused pulse in terms of C_3 reads as

$$C^\varepsilon_{tr}(\tau) = C_3(z(\frac{L}{\varepsilon^2}), \tau + t_1 + \frac{L}{\varepsilon^2} - z(\frac{L}{\varepsilon^2})) + O(\varepsilon).$$

Remember also that

$$g^\varepsilon(\tau) = -B_2(z(\frac{L}{\varepsilon^2}), \frac{L}{\varepsilon^2} - z(\frac{L}{\varepsilon^2}) + t_1 - \tau)G_{t_0,t_1}(t_1 - \tau) + O(\varepsilon).$$

We then shift and invert C_3:

$$C_4(z,\tau) = -C_3(z, t_1 + \frac{L}{\varepsilon^2} - z(\frac{L}{\varepsilon^2}) - \tau).$$

C_4 satisfies

$$C_4(z,\tau) = g_4^\varepsilon(\tau) - \frac{\varepsilon^2}{32}\int_0^z\int_\tau^\infty \Big[h'(z(\frac{L}{\varepsilon^2}) - y)\times$$
$$h'(z(\frac{L}{\varepsilon^2}) - y + \frac{\tau - s}{2})C_4(y - \frac{s}{2}, s)\Big]\, dsdy$$
$$-\varepsilon^2\frac{3\alpha_0}{4}\int_0^z C_4\frac{\partial C_4}{\partial\tau}(y,\tau)dy + O(\varepsilon), \tag{60}$$

where

$$g_4^\varepsilon(\tau) = B_2(z(\frac{L}{\varepsilon^2}),\tau)G_{t_0,t_1}\left(z(\frac{L}{\varepsilon^2}) - \frac{L}{\varepsilon^2} + \tau\right) + O(\varepsilon).$$

The integral over s in Eq. (60) actually goes from τ to $t_1 + \frac{L}{\varepsilon^2} - z(\frac{L}{\varepsilon^2})$ because C_4 vanishes for $\tau > t_1 + \frac{L}{\varepsilon^2} - z(\frac{L}{\varepsilon^2})$. The refocused pulse in terms of C_4 reads as

$$C_{tr}^\varepsilon(\tau) = -C_4(z(\frac{L}{\varepsilon^2}), -\tau) + O(\varepsilon).$$

We can now apply the averaging theorem. We get that C_4 converges as $\varepsilon \to 0$ to $\tilde{C}_4$ solution of

$$\tilde{C}_4(z,\tau) = g(\tau) - \frac{1}{16}\int_0^z \Lambda^*\tilde{C}_4(y,\tau)dy + \frac{3\alpha_0}{4}\int_0^z \tilde{C}_4\frac{\partial\tilde{C}_4}{\partial\tau}(y,\tau)dy, \tag{61}$$

where the function g is

$$g(\tau) = \tilde{B}_0\left(L, \tau - \frac{\phi_0(0)}{8}L\right)G_{t_0,t_1}\left(\tau + \frac{\sqrt{b_0(0)}}{\sqrt{2}}W_L + \frac{\phi_0(0)}{8}L\right) \tag{62}$$

and the operator Λ^* is

$$\Lambda^* f(\tau) = \frac{1}{2}\int_0^\tau \phi_1(-\frac{s}{2})f(\tau - s)ds = \left[\frac{1}{2}\phi_1\left(-\frac{\cdot}{2}\right)\mathbf{1}_{[0,\infty)}(\cdot)\right] * f(\tau). \tag{63}$$

In the Fourier domain

$$\int_{-\infty}^\infty \Lambda^* f(\tau)e^{i\omega\tau}d\tau = \overline{b_1(2\omega)}\int_{-\infty}^\infty f(\tau)e^{i\omega\tau}d\tau. \tag{64}$$

Accordingly,

$$\frac{\partial\tilde{C}_4}{\partial z} = \frac{\phi_0(0)}{8}\frac{\partial\tilde{C}_4}{\partial\tau} + \mathcal{L}^*\tilde{C}_4 - \frac{3\alpha_0}{4}\tilde{C}_4\frac{\partial\tilde{C}_4}{\partial\tau}, \tag{65}$$

where

$$\mathcal{L}^* = \mathcal{L}_r - \mathcal{L}_i. \tag{66}$$

The refocused pulse C_{tr}^{ε} also converges to

$$\tilde{C}_{tr}(\tau) = -\tilde{C}_4(L, -\tau). \tag{67}$$

Performing a final time shift allows us to state the following proposition.

Proposition 5.1 *The refocused pulse C_{tr}^{ε} converges as $\varepsilon \to 0$ to*

$$\tilde{C}_{tr}(\tau) = -\tilde{C}_0(L, -\tau), \tag{68}$$

where

$$\frac{\partial \tilde{C}_0}{\partial z} = \mathcal{L}_r \tilde{C}_0 - \mathcal{L}_i \tilde{C}_0 - \frac{3\alpha_0}{4} \tilde{C}_0 \frac{\partial \tilde{C}_0}{\partial \tau}, \tag{69}$$

$$\tilde{C}_0(0, \tau) = \tilde{B}_0(L, \tau) G_{t_0, t_1}(\tau + T_d), \tag{70}$$

$$T_d = \frac{\sqrt{b_0(0)}}{\sqrt{2}} W_L + \frac{\phi_0(0)}{4} L, \tag{71}$$

$$\frac{\partial \tilde{B}_0}{\partial z} = \mathcal{L}_r \tilde{B}_0 + \mathcal{L}_i \tilde{B}_0 + \frac{3\alpha_0}{4} \tilde{B}_0 \frac{\partial \tilde{B}_0}{\partial \tau}, \tag{72}$$

$$\tilde{B}_0(0, \tau) = f(\tau), \tag{73}$$

and the pseudo-differential operators $\mathcal{L}_r$ and $\mathcal{L}_i$ are defined by Eqs. (47-48).

5.3 Random linear case

In this subsection we assume that the nonlinear parameter $\alpha_0 = 0$. This case is already known in the white noise case [13], so we shall just remember the reader with this result and also extend it to the colored case. Taking the Fourier transform in Eqs. (69-72) yields that the transmitted pulse is

$$\tilde{B}(t) = K_{ODA}(t - T_d), \tag{74}$$

where the convolution kernel K_{ODA} has Fourier transform

$$\hat{K}_{ODA}(\omega) = e^{-\frac{b_r(2\omega)\omega^2 L}{4}} e^{-\frac{i b_i(2\omega)\omega^2 L}{4}}. \tag{75}$$

The refocused pulse is

$$-\tilde{C}_{tr}(-t) = \frac{1}{2\pi}\int\int e^{-i\omega t}e^{-\frac{b_0(2\omega)\omega^2 L}{4}-\frac{\overline{b_0(2\omega')}\omega'^2 L}{4}}e^{-i(\omega-\omega')T_d} \times\hat{G}_{t_0,t_1}(\omega-\omega')\hat{f}(\omega')d\omega' d\omega$$

where $\hat{G}_{t_0,t_1}$, resp. $\hat{f}$, is the Fourier transform of G_{t_0,t_1}, resp. f. If the front is completely recorded, then we can substitute 1 for G_{t_0,t_1} and δ_0 for $\hat{G}_{t_0,t_1}$, so that the refocused pulse is:

$$-\tilde{C}_{tr}(-t) = K_{tr} * f(t) \tag{76}$$

where the convolution kernel has Fourier transform

$$\hat{K}_{tr}(\omega) = e^{-\frac{b_r(2\omega)\omega^2 L}{2}}. \tag{77}$$

The important statement is that the contribution of the random time delay and of the effective dispersion $\mathcal{L}_i$ have been canceled by the time reversal, but the contribution of the effective diffusion $\mathcal{L}_r$ has been multiplied by 2.

5.4 Homogeneous nonlinear case

In the homogeneous case, the dynamics of the pulses $\tilde{B}_0$ and $\tilde{C}_0$ are governed by the inviscid Burgers equations:

$$\frac{\partial\tilde{C}_0}{\partial z} = -\frac{3\alpha_0}{4}\tilde{C}_0\frac{\partial\tilde{C}_0}{\partial\tau}, \tag{78}$$

$$\tilde{C}_0(0,\tau) = \tilde{B}_0(L,\tau)G_{t_0,t_1}(\tau), \tag{79}$$

$$\frac{\partial\tilde{B}_0}{\partial z} = \frac{3\alpha_0}{4}\tilde{B}_0\frac{\partial\tilde{B}_0}{\partial\tau}, \tag{80}$$

$$\tilde{B}_0(0,\tau) = f(\tau). \tag{81}$$

These equations can be solved by the characteristics method [8]. If $L < L_{shock}$

$$L_{shock} = \frac{4}{3\alpha_0}\min_{\tau, f'(\tau)>0}\left\{\frac{1}{f'(\tau)}\right\},$$

then the forward equation (80) has a well-defined solution $\tilde{B}_0$ which satisfies for any τ:

$$\tilde{B}_0\left(L, \tau - \frac{3\alpha_0}{4}f(\tau)L\right) = f(\tau).$$

Similarly, if $L < L_{shock,2}$,

$$L_{shock,2} = \frac{4}{3\alpha_0} \min_{\tau, g'(\tau)>0} \left\{ -\frac{1}{g'(\tau)} \right\}, \qquad g(\tau) = \tilde{B}_0(L,\tau) G_{t_0,t_1}(\tau),$$

then the backward equation (78) has a well-defined solution $\tilde{C}_0$ which satisfies for any τ':

$$\tilde{C}_0 \left(L, \tau' + \frac{3\alpha_0}{4} \tilde{B}_0(L,\tau') G_{t_0,t_1}(\tau') L \right) = \tilde{B}_0(L,\tau') G_{t_0,t_1}(\tau').$$

Choosing $\tau' = \tau - \frac{3\alpha_0}{4} f(\tau) L$ in the last equation:

$$\tilde{C}_0 \left[L, \tau + \frac{3\alpha_0}{4} f(\tau) \left(G_{t_0,t_1}(\tau - \frac{3\alpha_0}{4} f(\tau) L) - 1 \right) L \right] = f(\tau) G_{t_0,t_1}(\tau - \frac{3\alpha_0}{4} f(\tau) L).$$

Accordingly, if τ is such that $G_{t_0,t_1}(\tau - \frac{3\alpha_0}{4} f(\tau) L) = 1$, then $\tilde{C}_0(L,\tau) = f(\tau)$.

In the particular case where the front is completely recorded, then $L_{shock,2} = L_{shock}$ and $L < L_{shock} \Longrightarrow \tilde{C}_0(L,\cdot) \equiv f$. In the homogeneous case, either the propagation distance is smaller than the shock distance, and then time reversal completely rebuilds the initial pulse shape. Or the propagation distance is larger than the shock distance, and then time reversal completely fails as there is no uniqueness of the solution.

5.5 Random nonlinear case

To simplify the analysis we shall assume the white noise approximation and take $b_0(\omega) \equiv b_0$. We also consider that we completely record the transmitted front pulse. In this configuration, applying the Cole-Hopf transformation [8], we get a closed-form expression for the refocused pulse:

$$-\tilde{C}_{tr}(-t) = -\frac{2b_0}{3\alpha_0} \left[\ln \left(\int_{-\infty}^{\infty} \frac{e^{-\frac{(s-t)^2}{b_0 L}}}{\int_{-\infty}^{\infty} e^{\frac{3\alpha_0}{2b_0} \int_0^{s'} f(s'')ds''} e^{-\frac{(s-s')^2}{b_0 L}} ds'} ds \right) \right]_t \tag{82}$$

where $[\cdot]_t$ stands for a differentiation with respect to t.

Consider figures 3-5. We address cases where the transmitted pulse is strongly affected by nonlinearity. In particular the dot-dashed lines in figures 3a-4a-5a plot the transmitted pulse shapes in absence of randomness computed from the characteristics method, which show that a shock would have arisen before

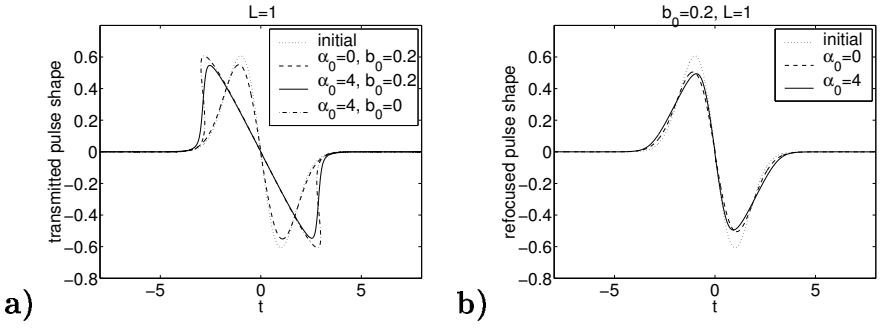

Fig. 3. Transmitted pulse shape $\tilde{B}_0(L,\cdot)$ (picture a) and refocused pulse shape $-\tilde{C}_{tr}(-\cdot)$ (picture b). We assume that the front pulse is completely recorded. The initial pulse is the derivative of a Gaussian $f(t) = -t\exp(-t^2/2)$. We compare the nonlinear configuration $\alpha_0 = 4$ with the corresponding linear configuration $\alpha_0 = 0$. The parameter $b_{\equiv}0.2$.

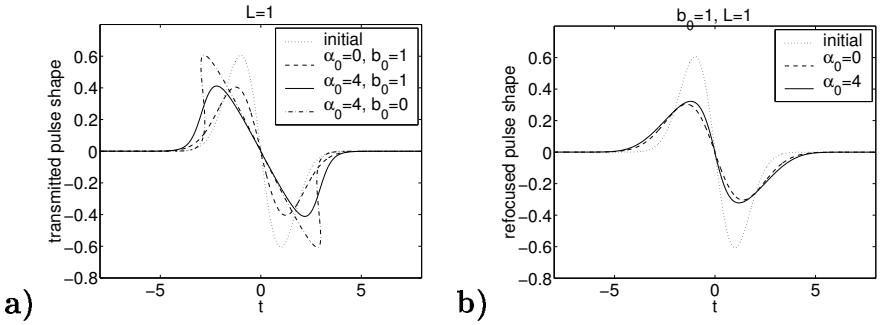

Fig. 4. Transmitted pulse shape $\tilde{B}_0(L,\cdot)$ (picture a) and refocused pulse shape $-\tilde{C}_{tr}(-\cdot)$ (picture b). The same as in figure 3, but we consider here stronger fluctuations $b_0 = 1$.

reaching the mirror. In such configurations refocusing by time reversal cannot be achieved as uniqueness of the solution is lost. In presence of randomness the effective diffusion prevents from shock formation (solid lines, figures 3a-4a-5a). It then appears that the time reversal process succeeds in compensating for the nonlinear effect (solid lines, figures 3b-4b). We should consider strongly nonlinear cases to detect a noticeable departure between the refocused pulse shapes in the linear and nonlinear cases, which appears as a steepening (solid line, figure 5b).

6 Numerical experiments

In this section we will illustrate the results obtained in the previous sections by performing full numerical simulations. We start by describing the numerical setup for the computer simulations regarding time-reversal in transmission (TRT). The code used is for a three-dimensional shallow water system [5]. For one-dimensional experiments the following reduced (one vertical layer system)

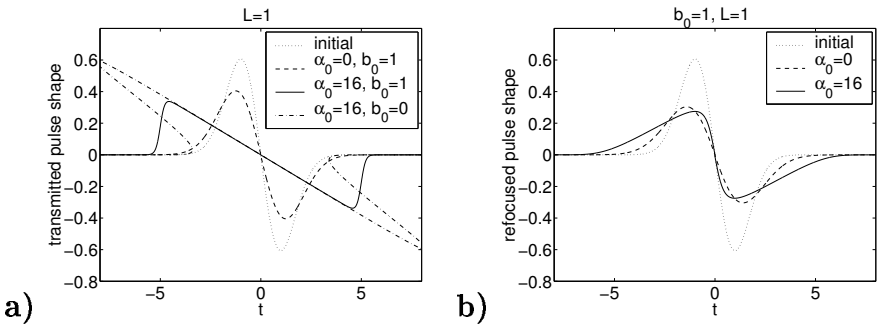

Fig. 5. Transmitted pulse shape $\tilde{B}_0(L,\cdot)$ (picture a) and refocused pulse shape $-\tilde{C}_{tr}(-\cdot)$ (picture b). The same as in figure 3, but we consider here stronger fluctuations $b_0 = 1$ and a stronger nonlinearity $\alpha_0 = 16$.

is utilized, for which the lateral velocity V will always be zero.

6.1 Numerical setup

The shallow water equations used in the numerical simulations are of the form

$$U_t + UU_x + VU_y = -g\eta_x \tag{83}$$

$$V_t + UV_x + VV_y = -g\eta_y \tag{84}$$

$$\eta_t + [HU]_x + [HV]_y = 0, \tag{85}$$

where the body of fluid is described by

$$H(x,y,t) = \eta(x,y,t) + h(x/\varepsilon, y).$$

Since the code is in dimensional variables we control nonlinearity through the amplitude of our initial data and the background (average) depth h_0. Nonlinearity corresponds to the amplitude-to-depth ratio α. To normalize the shallow water speed we choose our parameters so that it is equal to one in the flat regions: namely we set $g = 1/h_0$ so that $(gh_0) = 1$. Several linear validation experiments were presented in [12,18,19] and the numerical solution exhibited very good conservation properties over large propagation distances.

Equations (83–85) are discretized by an implicit, semi–Lagrangian technique which accomplishes the objective that the stability of the scheme does not depend on the celerity. A fixed staggered grid is defined on the horizontal plane. For the present one-dimensional experiments we have three lines of grid points along the horizontal direction, of which only the middle one is relevant [5,12]. It runs through the middle of the one-dimensional channel.

The other two are used for lateral boundary conditions. By a semi-Lagrangian technique we mean that the numerical transport is performed in an Eulerian–Lagrangian manner, relying therefore on the interpolation of the respective grid point–values at the backward–characteristic points of departure. Details are given in Casulli and Cheng [5] and the references within.

Recently this numerical scheme was thoroughly tested in the presence of a random medium and compared to theoretical **linear** O'Doherty-Anstey results [19]. It was also thoroughly tested for linear time-reversal in reflection [12], where the nonlinear study was initiated. In all simulations the initial pulse is given by the derivative of a Gaussian

$$\eta(x,0) = U(x,0) = -10\alpha\ (x - x_{j0})\ \exp\left(\frac{-(x-x_{j0})^2}{0.08}\right) \tag{86}$$

and is centered at node x_{j0}. Its effective width is equal to one.

6.2 Homogeneous nonlinear recompression

Nonlinear 1D acoustic (laboratory) experiments were reported by Tanter *et al.* [23]. An interesting fact mentioned in [23], concerns the difficulty to carry out laboratory experiments, "for very broadband signals, would require transducers with a huge bandwidth" which makes the experiments a "near impossible task". Hence the initial condition in [23] was a monochromatic sinusoidal wave. The pulse utilized in our numerical simulations is broadband. The nonlinear mechanism for energy transfer to the higher harmonic components during forward propagation is precisely the point investigated by Tanter *et al.* [23] in their laboratory experiments. The main goal of their experiments is to check for the reversibility of the energy transfer. The laboratory experiments are carried out for a nonlinear sinusoidal wave propagating in a homogeneous medium. The energy reversibility among harmonics is broken only for propagation longer than the shock formation distance. This shock distance corresponds to the critical time t_c calculated from Burgers equation. Consider Burgers equation $u_t + uu_x = 0, \qquad u(x,0) = \alpha\ h(x)$. Clearly $t_c = -1/(\alpha\ h'(x_c))$. In the simulations we will consider waves of the form

$$h(x) = -10x\ \exp\left(\frac{-x^2}{0.08}\right).$$

In this case $t_c = 1/(10\alpha)$, corresponding to the point with the largest negative slope ($x_c = 0$).

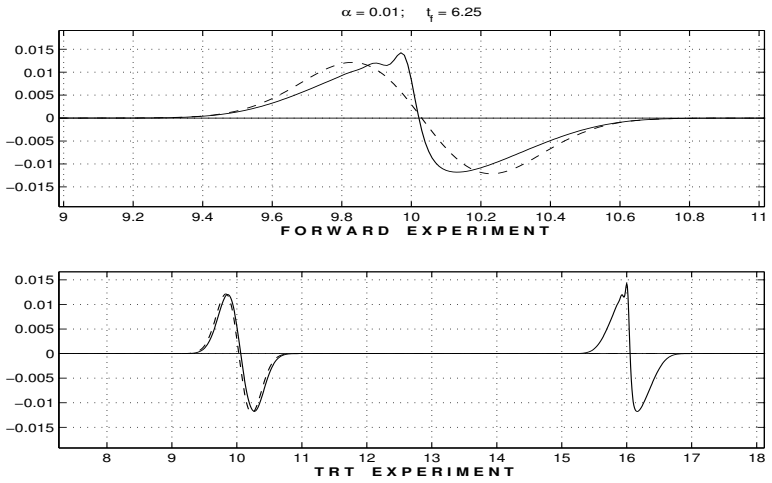

Fig. 6. TRT over a flat channel. Top: Initial condition (dashed line) and numerical solution (solid line) for $\alpha = 0.01$. The critical time is $t_c = 10$ and the computed time was $t = 6.25$. Bottom: to the right is the time-reversed wave elevation. To the left is the refocused wave (solid line) and the initial profile (dashed line).

In our first experiment we illustrate nonlinear time reversal in a homogeneous medium. As will be shown this amounts to energy recompression in Fourier space, namely an inverse cascading of energy from higher wavenumbers up to lower wavenumbers.

We solve the nonlinear shallow water system (83–85) in a flat channel (i.e. a homogeneous medium) with initial condition (86) ($\alpha = 0.01$; $x_{j0} = 10$). At critical time $t_c = 10$ a shock will form. With $\Delta x = 0.01$ and $\Delta t = 0.0025$ we are able to propagate numerically our pulse all the way up to $t = 6.25$ before spurious oscillations arise due to the mesh coarsening along the steep front. Increasing the resolution we can go further in time. The steep front (at time $t = 6.25$) is presented in the top part of figure 6 where it was shifted for comparison with the initial profile (centered at x_{j0}). The steep profile is time-reversed, propagated backward and it "refocuses" at the origin x_{j0} as seen at the bottom part of figure 6. There is no inhomogeneity and therefore no multiple scattering. Here refocusing (or recompression) should be understood in Fourier space. In figure 7 we can see the cascading of energy in Fourier space through the generation of higher harmonics due to nonlinear interaction. At the end of the forward simulation the Fourier spectrum is about 5 times broader that at $t = 0$ (solid line). After time reversion the back propagated pulse is such that the Fourier spectrum recompresses back to its narrower band (dashed line coinciding with solid line). This experiment is of the same nature as in [23] but for a broadband initial data.

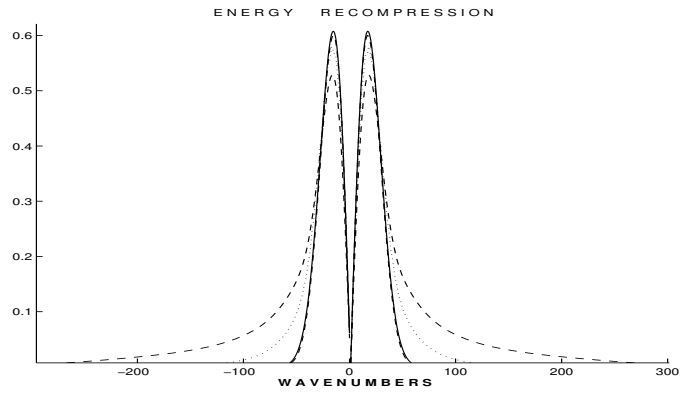

Fig. 7. At the center (solid line) we have the absolute value of the Fourier amplitudes for the initial data: $|\widehat{\eta(x,0)}|$. The generation of higher harmonics is depicted by the dotted line, which represents the spectrum at $t = 3.0$, and by the dashed line (at the final time $t = 6.25$). The Fourier spectrum of the time-reversed data is the wider dashed line and the spectrum of the refocused pulse is represented by the dashed line coinciding with the solid line.

6.3 The O'Doherty-Anstey theory and apparently viscous shocks

Now we consider inhomogeneous (disordered) media. The influence of the topography is felt through the depth function $H(x, y, t)$. The disordered medium is constructed by sampling a given number of random heights which are allocated at the one-dimensional mesh points. The correlation length of the disordered medium is represented by $\epsilon = m\Delta x, \quad m \geq 1$, in the simulations. These random heights are then connected by straight lines to form the synthesized topography. The channel has a total length of L units while the disordered topography covers only part of it (c.f. figure 8). In the following experiments we use the mesh $\Delta x = 0.0025$, $\Delta y = 0.1$ and $\Delta t = 0.000625$. These discretization parameters were chosen in order to get the desired accuracy and proper physical behavior when the nonlinear pulse interacts with the rapidly varying random medium ($\epsilon = 0.01$). Note that in this case $m = 4$. The fluctuations are 60% of the average depth in all experiments throughout this paper. These values were adjusted so that we could capture the desired features of the analysis, such as the apparent viscosity of the effective Burgers equation in section 4. In particular we want to capture the viscous shock profile. They were not chosen due to stability requirements. We set $\alpha = 0.004$ through the initial data which leads to $t_c = 25$. We chose this value so that we can propagate the inviscid Burgers solution for a longer time interval (than in the previous example) and compare it with its corresponding viscous profile as presented in figure 9. The waves have propagated about 18 units and the inviscid profile is steep. We clearly see the viscous shock due to the stochastic forcing.

To emphasize this viscous shock (stochastic) mechanism the evolution of the nonlinear wavefront is observed at different times. They are centered about

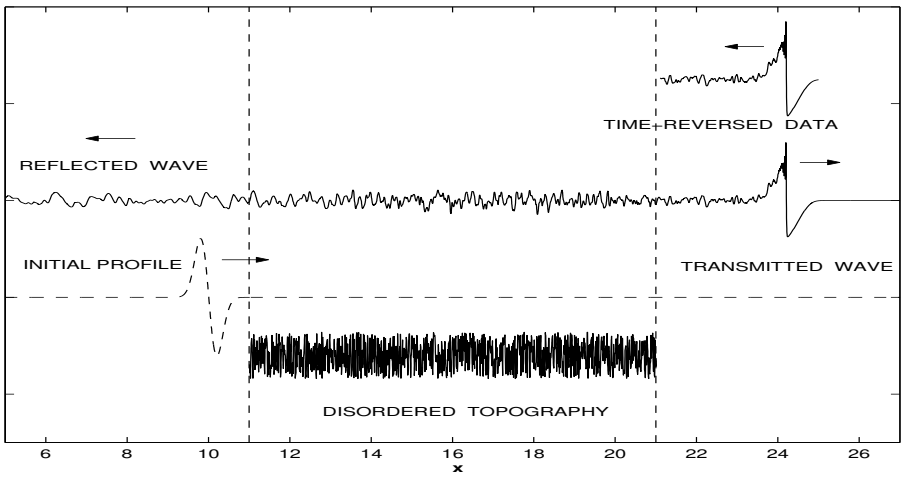

Fig. 8. The setup for the numerical simulations.

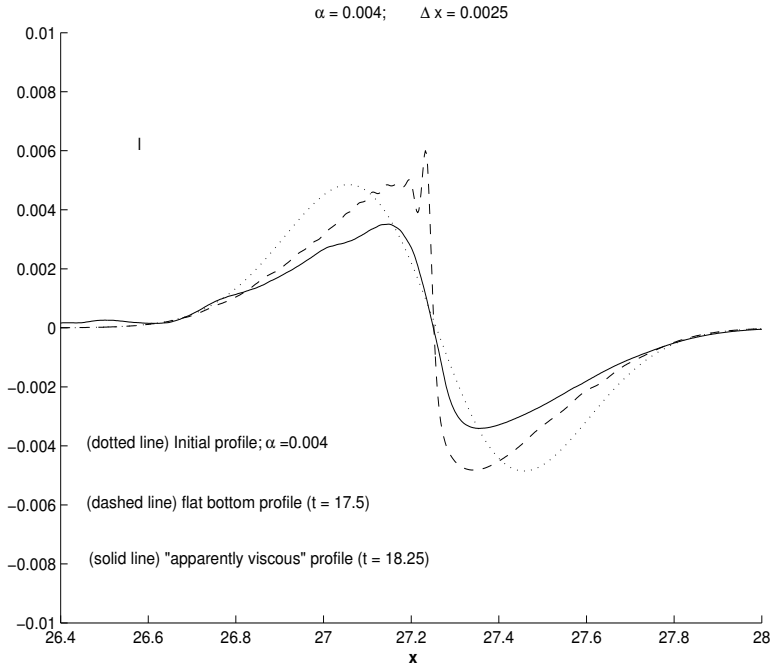

Fig. 9. The dashed line represents the inviscid (flat bottom) solution and the solid line the "apparently viscous" solution in the presence of a disordered topography. The inviscid solution was slightly shifted for a better comparison of the slopes. The dotted line represents the initial profile.

the solution at $t = 6.25$ in figure 10. Over a flat bottom the pulse continuously steepens under the "Burgers-like" nonlinearity (bottom of figure 10). In the presence of the stochastic forcing, promoted by the disordered topography, the dynamics is effectively governed by a viscous Burgers equation of the form $u_t + uu_x = \nu u_{xx}$, $u(x,0) = \alpha h(x)$ as presented earlier. A complete analysis of the viscous shock structure is presented in Whitham [24] (Chapter 4; in particular section 4.4). The shock structure scales according to the R^{-1}, where

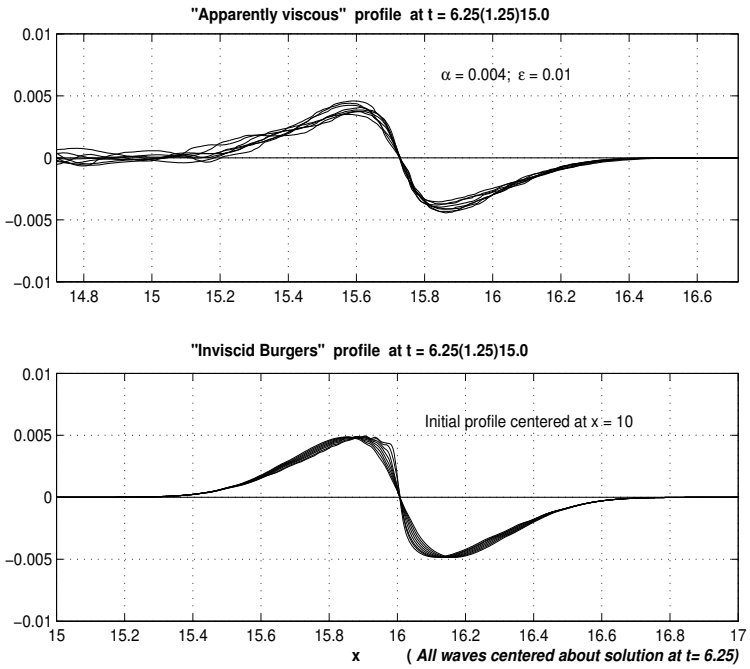

Fig. 10. "Apparently viscous" profile (top) and inviscid profile (bottom) at 8 different instants in time (with intervals equal to 1.25), all centered about the solution at $t = 6.25$.

this Reynolds number is defined as $R = \alpha/(2\nu)$. Moreover after the viscous shock reaches its limiting $O(R^{-1})$ transition layer a traveling wave arises as indicated in Whitham [24] (section 4.3). At the top of figure 10 the traveling wavefront regime (effectively speaking) can be clearly observed. The wavefront ceases to steepen and saturates on a given scale. We have verified numerically that for increasing values of α the front saturates at a smaller R^{-1} value, while increasing the ϵ of the disorder the slope becomes milder: larger correlation lengths imply in larger effective viscosity ν.

6.4 Nonlinear time reversal in transmission

In this section we illustrate time-reversal in transmission for a pulse that has propagated beyond its critical distance. We let $\alpha = 0.01$ which implies that $t_c = 10$. In figure 11 we have the initial profile to the left and two time-reversed data to our right (shifted above the free surface for better visualization). The time-reversed profiles were recorded at $t = 13.75$ and $t = 15$ both greater than t_c. As discussed above we have a viscous shock steeper than those presented in figure 10 because nonlinearity has been increased. But we are not in the situation described by Tanter *et al.* [23] because our wavefront developed into a viscous shock structure and not into a discontinuity, as in [23]. The time-reversed profiles are back-propagated into the disordered medium and refocus at the origin $x_{j0} = 10$ as expected. We can not tell the difference between the

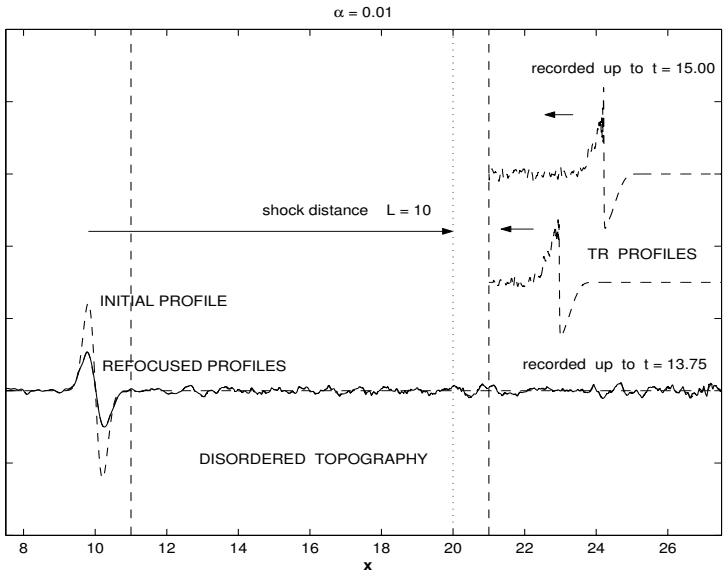

Fig. 11. Refocusing beyond the shock distance (vertical dotted line). The initial profile (dashed line) is to the left and two time-reversed data are to the right (shifted above the free surface for better visualization). The time-reversed profiles are back-propagated into the disordered medium and refocus at the origin $x_{j0} = 10$ at $t = 13.75$ and $t = 15$ respectively.

two refocused profiles.

7 Conclusion

In this paper we have addressed the propagation of nonlinear water waves in a disordered one-dimensional topography. In the presence of properly scaled stochastic forcing the solution is regularized leading to a viscous shock profile which depends on the degree of nonlinearity and on the power spectral density of the random fluctuations of the bottom. We have actually shown that the transmitted wave is governed by an effective viscous Burgers equation. We have also considered time-reversal problems and shown that the regularization effect allows us to extend the reversibility of the dynamics beyond the shock critical time.

We believe that these results can be extended to other nonlinear systems. For instance, the gas dynamics equation, or the nonlinear acoustic equation [23], can be written directly from the shallow water equations if we consider a polytropic gas with adiabatic exponent equal to two [24]. We believe that nonlinear systems that support Riemann invariants are likely to behave qualitatively like the model addressed in our paper.

References

[1] M. Asch, W. Kohler, G. Papanicolaou, M. Postel, and B. White, Frequency content of randomly scattered signals, *SIAM Review* **33** (1991), pp. 519-626.

[2] L. Berlyand and R. Burridge, The accuracy of the O'Doherty-Anstey approximation for wave propagating in highly disordered stratified media, *Wave Motion* **21** (1995), pp. 357-373.

[3] R. Burridge and H. W. Chang, Multimode one-dimensional wave propagation in a highly discontinuous medium, *Wave Motion* **11** (1989), pp. 231-249.

[4] R. Burridge, G. Papanicolaou, and B. White, One-dimensional wave propagation in a highly discontinuous medium, *Wave motion* **10** (1988), pp. 19-44.

[5] V. Casulli and R. T. Cheng, Semi-implicit finite difference methods for three-dimensional shallow water flow, *Int. J. Num. Meth. Fluids* **15**, (1992), pp. 629-648.

[6] J.-F. Clouet and J.-P. Fouque, Spreading of a pulse traveling in random media, *Annals of Applied Probability* **4** (1994), pp. 1083-1097.

[7] J.-F. Clouet and J.-P. Fouque, A time-reversal method for an acoustical pulse propagating in randomly layered media, *Wave Motion* **25** (1997), pp. 361-368.

[8] L. Debnath, Nonlinear partial differential equations for scientists and engineers Birkhäuser, Boston, 1997.

[9] A. Derode, A. Tourin, J. de Rosny, M. Tanter, S. Yon, and M. Fink, Taking advantage of multiple scattering to communicate with time reversal antennas, *Phys. Rev. Lett.* **90** (2003), 014301.

[10] M. Fink, Time-reversed acoustics, *Scientific American*, November 1999, pp. 67-93.

[11] M. Fink, G. Montaldo, and M. Tanter, Time reversal acoustics in biomedical engineering, *Annual Review of Biomedical Engineering* **5** (2003), pp. 465-497.

[12] J.-P. Fouque and A. Nachbin, Time-reversed refocusing of surface water waves, accepted for publication at *SIAM Multiscale Modeling and Simulation*, 2003.

[13] J.-P. Fouque and K. Sølna, Time-reversal aperture enhancement, *SIAM Multiscale Modeling and Simulation* **1** (2003), pp. 239-259.

[14] R. Z. Khasminskii, A limit theorem for solutions of differential equations with random right hand side, *Theory Probab. Appl.* **11** (1966), pp. 390-406.

[15] P. Lewicki, Long-time evolution of wavefronts in random media, *SIAM J. Appl. Math.* **54** (1994), pp. 907-934.

[16] -P. Lewicki, R. Burridge, and G. Papanicolaou, Pulse stabilization in a strongly heterogeneous medium, *Wave Motion* **20** (1994), pp. 177-195.

[17] J. C. Muñoz Grajales and A. Nachbin, Dispersive wave attenuation due to orographic forcing, submitted to *SIAM J. Appl. Math.*.

[18] A. Nachbin and V. Casulli, Water waves: linear potential theory results validated with a hydrostatic Navier-Stokes model, In: Mathematical and Numerical Aspects of Wave Propagation, Editor J. A. DeSanto, SIAM, 1998.

[19] A. Nachbin and K. Sølna, Apparent diffusion due to topographic microstructure in shallow waters, *Phys. Fluids*, **15**, (2003), pp. 66-77.

[20] R. F. O'Doherty and N. A. Anstey, Reflections on amplitudes, *Geophysical Prospecting* **19** (1971), pp. 430-458.

[21] C. Prada, E. Kerbrat, D. Cassereau, and M. Fink, Time reversal techniques in ultrasonic nondestructive testing of scattering media, *Inverse Problems* **18** (2002), pp. 1761-1773.

[22] K. Sølna, Focusing of time-reversed reflections, *Waves in Random Media* **12** (2003), pp. 365-385.

[23] M. Tanter, J. L. Thomas, F. Coulouvrat, and M. Fink, Breaking of time reversal invariance in nonlinear acoustics, *Phys. Rev. E* **64**, (2001) 016602.

[24] G. B. Whitham, Linear and nonlinear waves, John Wiley, 1974.